ACS NANO

www.acsnano.org

ARTICLE

Atomically Thin Two-Dimensional Kagome Flat Band on the Silicon Surface

Jae Hyuck Lee, Gwan Woo Kim, Inkyung Song, Yejin Kim, Yeonjae Lee, Sung Jong Yoo, Deok-Yong Cho, Jun-Won Rhim,* Jongkeun Jung,* Gunn Kim,* and Changyoung Kim*

Cite This: *ACS Nano* 2024, 18, 25535−25541

Read Online

ACCESS | Metrics & More | Article Recommendations | Supporting Information

ABSTRACT: **In condensed matter physics, the Kagome lattice and its inherent flat bands have attracted considerable attention for their prediction and observation to host a variety of exotic physical phenomena. Despite extensive efforts to fabricate thin films of Kagome materials aimed at modulating flat bands through electrostatic gating or strain manipulation, progress has been limited. Here, we report the observation of a d-orbital hybridized Kagome-derived flat band in Ag/Si(111) $\sqrt{3} \times \sqrt{3}$ as revealed by angle-resolved photoemission spectroscopy. Our findings indicate that silver atoms on a silicon substrate form an unconventional distorted breathing Kagome structure, where a delicate balance in the hopping parameters of the in-plane d-orbitals leads to destructive interference, resulting in double flat bands. The exact quantum destructive interference mechanism that forms the flat band is uncovered in a rigorous manner that has not been described before. These results illuminate the potential for integrating metal−semiconductor interfaces on semiconductor surfaces into Kagome physics, particularly in exploring the flat bands of ideal 2D Kagome systems.**

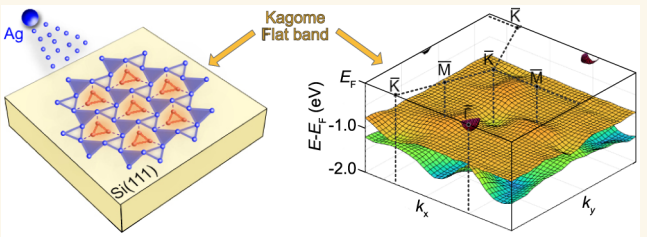

KEYWORDS: *silicon, two-dimensional, Kagome, flat bands, d-orbital, ARPES, DFT*

Kagome materials have captivated the scientific community because of their intriguing band topologies and potential for exotic quantum phenomena. These materials feature flat bands coexisting with Dirac points and van Hove singularities.[1] The flat band states are now drawing more attention due to the recent claims that they could be another underlying mechanism for heavy Fermionic behavior.[2] Despite a wealth of research on Kagome materials,[1−19] synthesizing or manipulating true *two-dimensional* Kagome lattices with ideal Kagome flat bands has proven challenging. Moreover, conventional Kagome materials that have been primarily researched for their flat bands have been limited to binary metal magnets T_mX_n (T = 3d TMs, X: Sn,Ge, and m:n = 3:1,3:2,1:1),[5−11] ternary magnets ($A(Mn,V)_6Sn_6$, $Co_3Sn_2S_2$),[1,12−16] van der Waals materials (AV_3Sb_5),[1,17] and a series of breathing Kagome chalcogenide halides.[18,19]

Traditional experimental methods such as exfoliation and molecular epitaxy are required to fully explore the 2D nature of Kagome materials. However, the synthesis and manipulation of high-quality two-dimensional samples, either in the form of single crystals or films, are challenging, which limit the progress in the study of low-dimensional Kagome systems,[20] which are often critical in creating dispersionless band structures for these frustrated lattices. To overcome these limitations, we introduce an approach to expand the horizons of 2D Kagome physics. Specifically, we fabricate atomically thin two-dimensional Kagome systems by depositing monolayers of metal atoms onto a semiconductor surface. We speculate that such a method has four significant advantages in that (1) surface reconstructed structure is inherently *two-dimensional*, (2) conventional semiconductors such as silicon or germanium are commercially widely available, and there has been a plethora of studies regarding the naturally induced surface reconstructed systems of these materials, (3) a semiconducting substrate does not contribute to the density of states near the Fermi level due to the band gap, which is important in identifying electronic and transport properties of the actual surface system, and (4) high degrees of freedom in surface engineering are provided by various deposition materials.[21−23]

As a representative example, we focus on the $\sqrt{3} \times \sqrt{3}$ surface reconstruction of Ag one monolayer on the Si(111) substrate, hereafter referred to as the Ag/Si system. This system has attracted significant attention due to the promising properties of the metal−silicon interface and its potential

Received: April 23, 2024
Revised: August 13, 2024
Accepted: August 14, 2024
Published: August 30, 2024

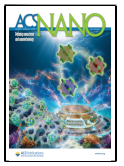

applications in electronics.[24−26] Although extensively studied, the precise nature of its structure was only recently resolved[25−31] as an "in-equivalent-trimer" (IET) configuration,[31] where the uppermost silver atoms form connected trimers of two different sizes [Figure 1a,b]. Intriguingly, we find that the IET configuration can be reinterpreted as a modified Kagome lattice. As illustrated in Figure 1c, a breathing Kagome lattice is essentially a deformed Kagome lattice with a broken inversion symmetry. The IET lattice can be seen as an even further distorted breathing Kagome lattice, where the smaller triangle rotates by 18° and the larger one rotates by 12° in the opposite direction. We term this structure as a distorted breathing Kagome (DBK) lattice.

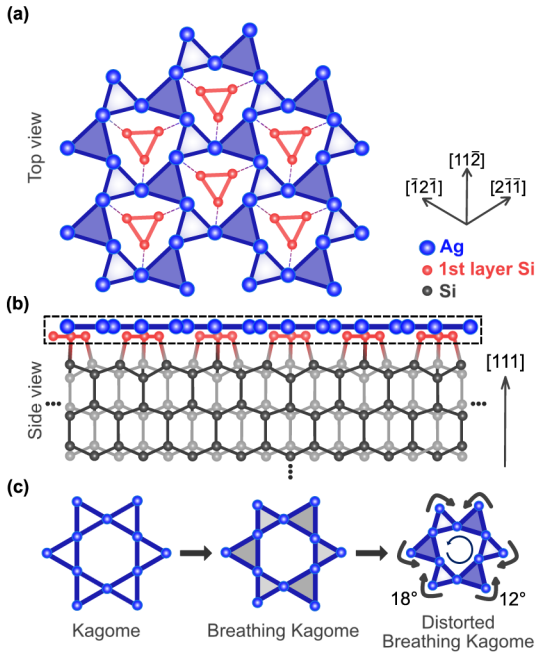

Figure 1. Atomic structure and schematic illustration of the Ag/Si system. (a) Top view and (b) side view of the Ag/Si system, respectively. Blue spheres represent Ag atoms, red spheres represent the uppermost Si atoms that form a trimer inside the distorted Ag hexagons, and black and gray spheres represent the bulk Si atoms. (c) Depiction of the distortions leading to the formation of the DBK, starting left from the basic Kagome model to the Kagome lattice with a breathing distortion and finally to the rotational distortion applied breathing Kagome lattice.

Using angle-resolved photoemission spectroscopy (ARPES), we confirm the presence of Kagome bands in the Ag/Si system. Subsequent density functional theory (DFT) and tight-binding (TB) calculations confirm the 2D nature of the Ag/Si system and elucidate the origin of the flat band. The band structure of the Ag/Si system is explained with a hybridized d-orbital Kagome model, consisting of double flat bands. Furthermore, we identify a compact localized state (CLS) of a hybridized d-orbital Kagome model, which is different from a conventional Kagome system, and the corresponding destructive interference mechanism from the hybridized d-orbital Kagome model is rigorously demonstrated. We also emphasize that this is the realization of a flat-band Kagome system on a Si substrate. From the discovery of a Kagome system on a surface reconstructed system, we carefully raise the possibility of an unconventional method for the study of two-dimensional Kagome systems on semiconductor surfaces, potentially contributing to a broader range of Kagome nanostructure research.

RESULTS AND DISCUSSION

Electronic Band Structure of the Ag/Si System. We first look into the electronic band structure through the ARPES results displayed in Figure 2a,b. Figure 2a is an APRES cut along the $\bar{\Gamma} - \bar{K} - \bar{M} - \bar{\Gamma}$ direction (taken along the thick line in Figure 2b), while Figure 2b displays the whole three-dimensional band structure of the Ag/Si system. The hexagonal reciprocal lattice matches the $\sqrt{3} \times \sqrt{3}$ surface structure. For both Figure 2a,b, binding energy (E_B) down to ≈−3 eV is plotted to show both Si bulk bands and Ag−Si surface states.[25] From Figure 2a,b, it is shown that there exist three surface bands; a nearly flat band (SF), a dispersive band just below the flat band (S1), and an electron pocket crossing E_F (S2), each represented by orange, green, and purple dotted lines, respectively. These surface bands were assigned as

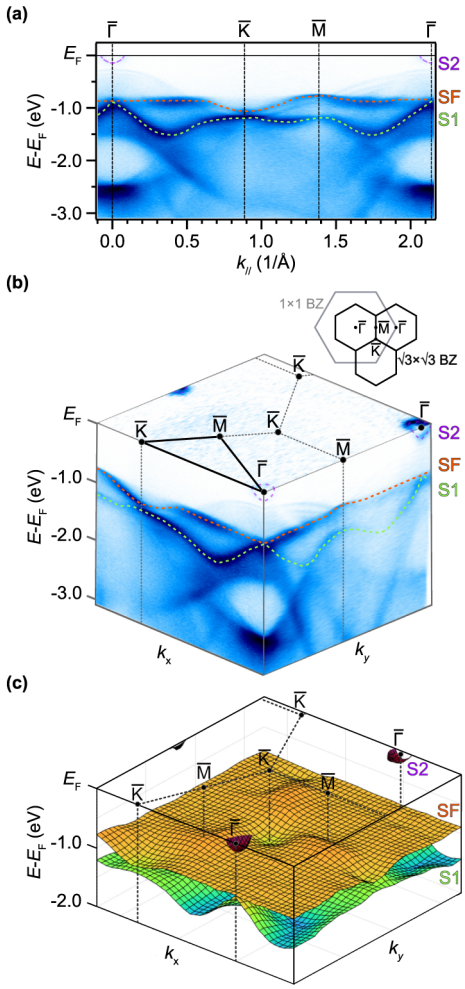

Figure 2. ARPES data of the Ag/Si system. (a) ARPES electronic band structure along the $\bar{\Gamma} - \bar{K} - \bar{M} - \bar{\Gamma}$ cut. (b) 3D ARPES plot of the Ag/Si system. The dotted gray lines represent the BZs with high-symmetry points denoted. The topmost surface represents the Fermi level (E_F). The three surface bands (S1, SF, and S2) are highlighted by green, orange, and purple dotted lines, respectively. (c) The three surface bands are fitted and interpolated from (b).

https://doi.org/10.1021/acsnano.4c05398
ACS Nano 2024, 18, 25535−25541

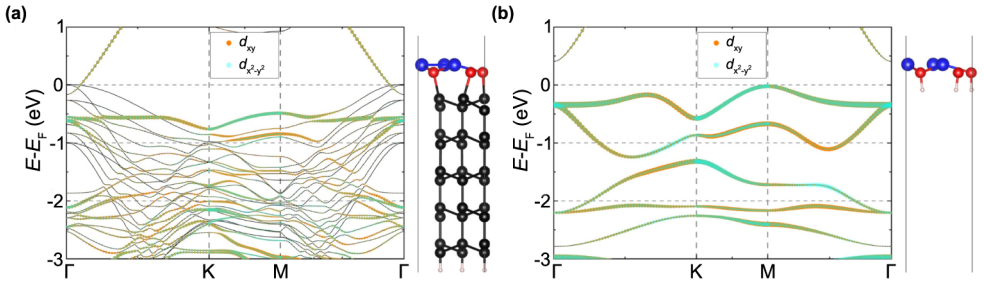

Figure 3. Layer-dependent DFT calculations. (a) Fat-band calculations for a hydrogen-terminated slab system with multilayer Si atoms. (b) The thickness of the slab system has been dramatically reduced, leaving only the topmost Si and Ag layer. On the left panels of (a,b), the fat-band calculations for the $4d_{xy}$ and $4d_{x^2-y^2}$ orbitals of Ag atoms are displayed. The orbital contributions of the $4d_{xy}$ and $4d_{x^2-y^2}$ orbitals of the Ag atoms are shown by the sizes of the orange and cyan circles, respectively. The side-views of the atomic structures for each of the slab systems are depicted in the right panels. Ag, topmost Si, bulk Si, and H atoms are represented by blue, red, black, and white spheres, respectively.

derived from the topmost Ag and Si atoms,[24,25,28] which will be verified by DFT calculations in the next section. Further TB calculations in the next section indicate that all three surface bands have their origins in the Ag Kagome lattice.

The SF and S1 bands are both located near a E_B of −1 eV. The SF band remains flat throughout most of the Brillouin zone (BZ) but shows dispersion ($\lesssim$ 0.15 eV) near the $\overline{K}$ point, as seen in the orange dotted line in Figure 2a,b. The broadening of the flat band near the $\overline{\Gamma}$ point is possibly due to hybridization with the weak hole-like bands that lie between S2 and SF at the $\overline{\Gamma}$ point. Near the BZ boundary, on the other hand, the flat band is located above the hole-like bands in the bulk-gap region, making it sharper. These weak but distinct hole-like bands are attributed to Si-related surface resonance bands, hole sub-bands in a Si quantum well, or both.[28,32]

In addition to the flat band, the ARPES result confirms another signature of a Kagome band: A quadratic band touching (QBT) at the $\overline{\Gamma}$ point, which is a key characteristic of a Kagome band structure.[3,33,34] A flat band having this type of QBT is called a singular flat band,[3] which is expected to show many exotic quantum geometric phenomena characterized by the quantum distance, such as the anomalous Landau levels[35] and the unconventional bulk-boundary correspondence.[36] We note that although there should be a spin−orbit coupling (SOC)-induced gap between SF and S1 at the $\overline{\Gamma}$ point, it is hard to identify within the resolution of the ARPES data due to band broadening near the $\overline{\Gamma}$ point. Moreover, the gap size is small (≈16 meV) due to the weak SOC strength of Ag [see Figure S2]. However, by replacing Ag with heavy elements with strong SOC, we expect to realize a nearly flat topological band.[35]

Finally, S2 forms an isotropic electron pocket with a minimum E_B of approximately −0.15 eV at the $\overline{\Gamma}$ point. This metallic S2 band forms a circular Fermi surface, indicating a two-dimensional free-electron-like surface state, and has been relatively well-studied compared to other surface bands.[24,37,38]

For clarity, only the three surface bands SF, S1, and S2 were fitted and extrapolated to surfaces for the whole BZ and are plotted in 3D in Figure 2c. The S2 electron pocket is revealed as the closed purple surface centered around the $\overline{\Gamma}$ point. As hinted in Figure 2a,b, the flat band of SF is clearly visualized across most of the BZ, with a small degree of dispersion on the zone boundary. The flatness and zone boundary dispersion of SF are directly realized by the surface color gradient of SF in Figure 2c, where the largest change is at the surface dip near the $\overline{K}$ point (scaling to $\lesssim$ 0.15 eV). The dispersion near the $\overline{K}$ point is driven by next-nearest-neighbor hopping, which is typically found in realistic Kagome models.[35] Compared to SF, S1 is highly dispersive and crosses SF only at the $\overline{\Gamma}$ point via QBT, which, we emphasize again, is of a Kagome nature. We would like to point out that the full BZ scan with a high resolution and the 3D mapping of the electronic band structure allow the realization of the flat band throughout the BZ and a clear assessment of QBT between SF and S2 in the Ag/Si system, which was not so apparent until now.

Origin of the Flat Band. *DFT Calculations.* To investigate the origin of the observed flat band in the Ag/Si system, we employed DFT calculations. Our computational model, which was carefully designed to match the experimental conditions, helped us map the flat bands to the atomic orbitals within the structure. The DFT results, displayed in Figure 3a, demonstrate excellent agreement with our ARPES data [see Figures S3 and S4]. The accuracy of our DFT calculations is shown by the fact that they were able to reproduce the three surface bands (SF, S1, and S2). Moreover, the hole sub-bands between the S2 and SF bands and bulk bands from the Si substrate are all present. However, it is difficult to understand the complex nature of these bands simply by looking at them. We need to use a more sophisticated approach.

Our analysis suggests that the flat bands likely originate from the surface of the material. Projected density of states (DOS) calculations reveal that the dominant contribution to the surface bands emanates from the in-plane Ag atomic orbitals, specifically the $4d_{xy}$ and $4d_{x^2-y^2}$ orbitals, shown in orange and cyan in Figure 3a,b, respectively. Additional contributions are observed from the Si p-orbitals. We note that while the results in ref.[24] suggest that the in-plane p-orbitals of the Ag atoms are the main contributors of the surface bands, our careful evaluation on projected DOS of Ag and Si in all layer models shows that the in-plane d-orbitals are the main contributors [see Figure S3].

To gain deeper insights into the complex interactions of these hybrid orbitals, we needed a simplified model. We therefore performed additional calculations with fewer layers of Si atoms to verify the primary contributions of the surface bands from the uppermost atoms, particularly the Ag atoms in the DBK lattice. This allowed us to focus only on the contributions from the Ag and Si atoms at the surface. Interestingly, when we kept the Ag layer and removed most of the silicon layers, flat bands remained. In contrast, the Si bulk

https://doi.org/10.1021/acsnano.4c05398
ACS Nano 2024, 18, 25535−25541

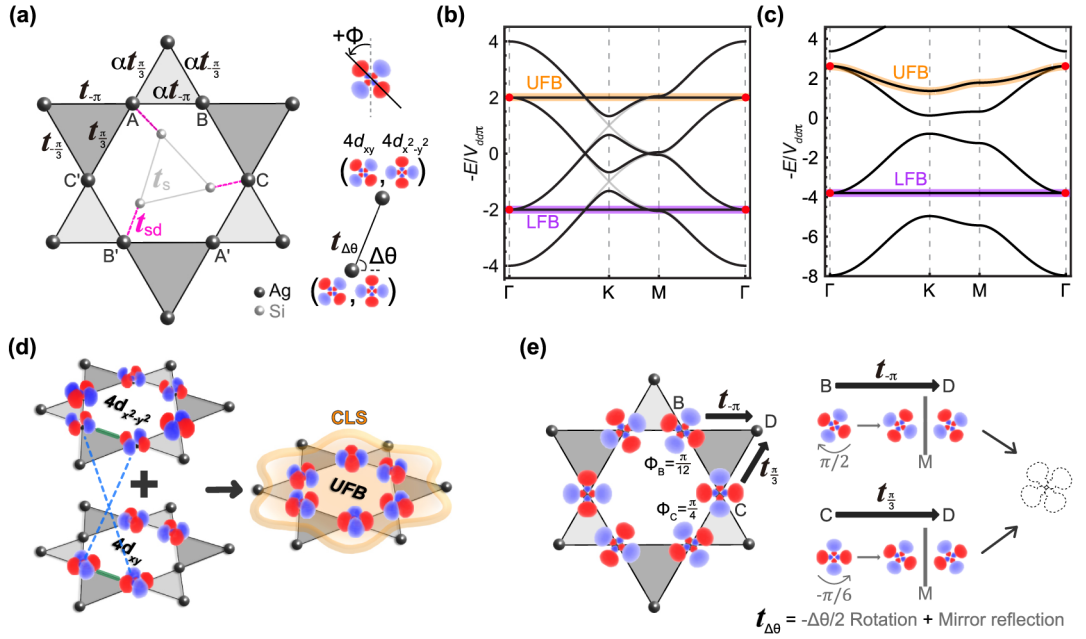

Figure 4. Origin of the flat band. (a) Schematic of the lattice structure of the Ag/Si system for TB calculation where the breathing Kagome lattice of Ag atoms couples with a Si triangle within its hexagon. The hopping matrices $t_{\Delta\theta}$ between Ag atoms are displayed together with the asymmetry parameter α. The gray lines represent the hopping between the topmost Si atoms (t_s), and the dotted magenta lines stand for the hopping between Ag and Si atoms (t_{sd}). The $t_{\Delta\theta}$ consists of intra- and inter-orbital hopping between $4d_{xy}$ and $4d_{x^2-y^2}$ (bottom-right schematic). ϕ represents the real rotation angle of the d_{xy} orbital (top-right schematic). (b) Band structure of the multiorbital Kagome lattice with $V_{dd\pi} = 1$, $E_0 = 0$, $\alpha = 1$ (light gray line), and $\alpha = 0.8$ (dark black line). (c) The recreated band structure of the Ag/Si system obtained from the band parameters $V_{dd\sigma}/V_{dd\pi} = V_{dd\delta}/V_{dd\pi} = -1$, $V_{sd}/V_{dd\pi} = 2$, $t_s/V_{dd\pi} = -1$, $\epsilon/V_{dd\pi} = 5$, and $\alpha = 2.8$. The UFB and LFB are each emphasized by orange and purple lines, respectively, with the QBT marked by a red dot. (d) Schematic of the orbital couplings leading to the formation of CLS in the multiorbital Kagome lattice ($\alpha = 0.8$). Intraorbital hopping and interorbital hopping between $4d_{xy}$ and $4d_{x^2-y^2}$ are each represented by solid green and broken blue lines, respectively. The orbital configuration of the UFB is exhibited, and its CLS is represented by the orange shaded hexagon. (e) Mechanism of destructive interference in the UFB.

and other bands disappeared, revealing a gapped Dirac band-like feature characteristic of a breathing Kagome lattice between −0.4 and −2.2 eV, as shown in Figure 3b. Notably, another flat band was observed at around −2.2 eV in the single-layer DFT calculation, intersecting the Dirac band at a QBT point. This additional flat band at −2.2 eV touches on the limitation of the single (s-)orbital Kagome lattice model in describing the d-orbital Kagome system and calls for attention of the "double" flat band as an indicator in identifying multiple d-orbital Kagome band structures.

Tracing the behavior of the Dirac-like band was difficult in our original model, because it interacted with the Si bulk band. However, by decreasing more Si layers [see Figure S3], we could see how the band evolved. Although the band changed slightly, the $4d_{xy}$ and $4d_{x^2-y^2}$ orbitals remained within the Kagome-like band, confirming that this band persisted and continued to be influenced by these Ag orbitals. Additionally, as we removed more Si layers, the orbital contributions to the flat bands shifted, further highlighting the importance of the in-plane Ag orbitals.

Tight-Binding Analysis and Origin of Surface Bands. To corroborate our layer-dependent DFT results and to elucidate the origin of the flat band with the destructive interference mechanism, we perform TB analysis on a generalized Kagome structure of the Ag/Si system, as illustrated in Figure 4a. We select only the Ag $4d_{xy}$, $4d_{x^2-y^2}$, and Si 3s orbitals as the basis of the TB Hamiltonian based on the DFT results. We introduce a vectorial representation $\mathbf{d} = (\alpha, \beta)$ for the linear combination of d-orbitals, $|\psi\rangle = \alpha|d_{xy}\rangle + \beta|d_{x^2-y^2}\rangle$. The combined state ψ can be denoted by an angle θ of $\mathbf{d}$ with respect to the x axis [lower right schematic in Figure 4a]. Note that the real rotation angle ϕ of the d_{xy} orbital is half of $-\Delta\theta$ [upper right schematic in Figure 4a]. For example, the $d_{x^2-y^2}$ orbital, corresponding to $\theta = \pi/2$, is rotated $\phi = -\pi/4$ from the d_{xy} orbital. Then, the hopping of d-orbitals ($\mathbf{d}$) to the neighboring sites at an angle $\Delta\theta$ is given by $t_{\Delta\theta} = V_{dd\pi}M_xR_{\Delta\theta}$, where $M_x = -\sigma_z$ corresponds to the mirror reflection with respect to the y axis ($x \rightarrow -x$) and $R_{\Delta\theta}$ is a rotation matrix. In our model, only three angles, $\Delta\theta = \pi/3, -\pi/3$, and $-\pi$, are used [left schematic in Figure 4a].

First, we ignore the Si atoms in Figure 4a ($t_{sd} = 0$ and $t_s = 0$) to account for only the DBK lattice of the Ag atoms. The band structures of ideal ($\alpha = 1$) and breathing ($\alpha = 0.8$) Kagome models are plotted in Figure 4b, where α is an asymmetry parameter between two triangles with different sizes. The breathing Kagome lattice is characterized by the gap opening at the K point due to the breaking of inversion symmetry.[18] However, for both cases, the upper flat band (UFB) and the lower flat band (LFB) persist, which are connected to the nearly flat bands found in the DFT and experimental results. Also, QBTs with the quadratic Dirac band at the Γ point, protected by the C_3 symmetry of the DBK lattice, are present for both cases.

Next, we turn on the coupling of the Ag d-orbitals to the Si s-orbital ($t_{sd} \neq 0$) and the hopping between Si ($t_s \neq 0$), to investigate the deformation of flat bands into nearly flat bands

https://doi.org/10.1021/acsnano.4c05398
ACS Nano 2024, 18, 25535−25541

of the realistic system. The overall characteristics of the electronic band still remain as follows: Both UFB and LFB exist along with the two Dirac bands between the energy range of the two flat bands [see Figures 4c and S9]. Note that the QBTs are also robustly conserved for both UFB and LFB at the Γ point due to the protected C_3 symmetry by the triangular Si lattice. This result is in parallel to the layer-dependent DFT band dispersion, which took into account only the topmost Ag and Si atoms in Figure 3b. While UFB remains flat near the Γ point, its dispersion becomes the largest at the K point, maintaining a gap between the Dirac band below. We note that, according to the TB analysis, the gap just above the UFB is found to be topologically trivial [see Figure S10].

The uppermost quadratic Kagome band in Figure 4b, on the other hand, undergoes a drastic change after the inclusion of Si orbitals, forming an isotropic electron pocket, mimicking the S2 band, as shown in Figure 4c. Such a modification of the band after the insertion of Si is in line with the previous interpretation that S2 is a surface state having bonding character of both Ag−Si orbitals.[24,25,37,38] The electron pocket is also evident in the topmost layer DFT calculation [Figure 3b].

Overall, we have shown that the most essential features of the ARPES band structure, such as the nearly flat bands, the free-electron-like band, and the QBT at the Γ point, are captured by the electronic structure of the topmost Ag and Si layer from DFT and TB analysis [compare Figures 2a, 3b, and 4c]. The similarities among the ARPES data, DFT, and TB calculations strongly suggest that the nearly flat bands originate from the Kagome structure of the Ag/Si system. Surprisingly, studies so far regarding hybridized d-orbital Kagome systems have not explicitly utilized the double-flat-band structure given in Figure 4b as applied here to the Ag/Si system. The reason such a double flat band of the hybridized d-orbital Kagome system is apparent in the Ag/Si system is because the Ag/Si system is a two-dimensional monolayer Kagome structure with relatively few interactions with other atoms, thus preventing significant disruption of the band structure.

Mechanism of the Destructive Interference. The origin of a flat band is understood from the existence of a nontrivial localized eigenstate CLS, which has finite amplitudes only inside a finite region due to destructive interference.[3,33] One of the most well-known CLSs is the hexagon-shaped one of the s-orbital Kagome lattice model.[39] While the Ag/Si system has also turned out to be a Kagome structure, we show that the mechanism behind the formation of a flat band is completely different from that of the popular s-orbital Kagome model. We demonstrate that the CLS of the Ag/Si system is stabilized by the interorbital destructive interference between two d-orbitals, as shown in Figure 4d. We note that these extremely localized eigenmodes experience the inverse Anderson localization[40] as defects are introduced [see Figure S11].

Let us see how the mixed d-orbitals at the B and C sites can be canceled out at the D site via destructive interference after the hopping processes. At B and C sites, θs for the orbital compositions of the CLS are given by $\theta_B = -\pi/6$ and $\theta_C = -\pi/2$ (or $\phi_B = \pi/12$ and $\phi_C = \pi/4$), respectively. After the hopping processes, d-orbitals at the B(C) site hop to the neighboring D site via $t_{-\pi}(t_{\pi/3})$, resulting in $\theta_B \rightarrow \theta_B + \Delta\theta = -7\pi/6$ or $\phi_B \rightarrow \phi_B + \Delta\phi = 7\pi/12$ ($\theta_C \rightarrow \theta_C + \Delta\theta = -\pi/6$ or $\phi_C \rightarrow \phi_C + \Delta\Phi = \pi/12$). That is, ϕ_B and ϕ_C become out of phase ($\pi/2$) at the D site after each hopping, implying that their linear combination vanishes and destructive interference is achieved.

Such a mechanism is consistent for CLSs in all multiple d-orbital-based (breathing) Kagome systems regardless of the minute distortion, as seen in the Ag/Si system [see Figure S12]. Thus, we have deduced the CLS corresponding to the flat band SF and elucidated the underlying quantum destructive interference typically present in Kagome systems.

Along with the perseverance of the overall double-flat-band structure, another interesting common feature between Figures 3b and 4c is that the LFB remains robustly flat compared to the UFB. This is because the CLS of the LFB remains the same even after the coupling with Si atoms is turned on. As shown in detail in Figure S8 and Eq 20 of Supporting Information, the amplitudes corresponding to the two d-orbitals of the LFB at the Ag atoms connected to the Si orbital have opposite signs with a ratio inversely proportional to the sd-coupling strength. Consequently, the d-orbitals cancel each other at the Si sites after hopping. This destructive interference condition remains robust against the distortion of the Ag triangles [see Figure S12]. However, when the Si triangles are distorted, the perfect destructive interference is disrupted, leading to the LFB transforming into a nearly flat band. Meanwhile, the QBT remains robust because the C_3 symmetry is still preserved [see Figure S13]. We note that the LFB is not apparent in the ARPES data, possibly because of overlap with the complex Si bulk band and the fact that features are generally not clear at high binding energies.

CONCLUSION

In summary, we have reinterpreted the Ag/Si system as a type of Kagome lattice with hybridized d-orbitals. Using ARPES, we have measured a flat band with a QBT at the $\overline{\Gamma}$ point in the surface-reconstructed Ag/Si system. DFT calculations confirm that the dominant orbital contribution of the flat band comes from the in-plane 4d-orbitals. Comparisons with TB calculations and DFT on the topmost atomic layers reveal that the double flat bands are multiorbital Kagome bands with quantum destructive interference resulting from a delicate balance between the interorbital hopping parameters and the distinctive bonding geometry from in-plane orbitals. This destructive interference is crucial for nontrivial CLS.

Furthermore, we propose that the UFB energy can be controlled via hole-doping. For flat bands to give rise to unconventional correlation phenomena, they must be close to the E_F. Indeed, when the Ag/Si system was grown on p-doped Si, we were able to confirm that the E_F is lowered by ≈0.1 eV compared to the one grown on n-doped Si [see Figure S14]. The area of the metallic electron pocket (S2) on the Fermi surface decreases when the substrate is changed from n-doped Si (0.77% of the BZ) to p-doped Si (0.14% of the BZ). By rough estimation using the Luttinger theorem, the electron concentration level decreases by 0.0126 electrons per unit cell when the substrate is changed to p-doped Si. Even with such a small amount of reduced electron concentration, the E_F shifts by 0.1 eV. We thus propose that further investigations of doping methods could bring the UFB closer to the E_F, allowing the realization of transport properties and applications.

METHODS

Sample Preparation and ARPES Measurements. Sample fabrication and ARPES measurements were conducted in a home-built in situ ARPES cluster system at Seoul National University

https://doi.org/10.1021/acsnano.4c05398
ACS Nano 2024, 18, 25535−25541

(SNU). The details of the fabrication process are given in Supporting Information. A He−Iα photon source ($h\nu$ = 21.2 eV) emitted from a discharge lamp (Fermion Instrument) was used, and the spectra were obtained at 10 K using a Scienta DA30 analyzer. Sample preparation, transfer, and measurement were all performed in an Ultra-High-Vacuum environment better than 5×10^{-11} Torr.

DFT Calculations. This study used the Vienna Ab initio Simulation Package (VASP) program to perform DFT calculations.[41,42] The projector-augmented wave (PAW) method[43] was used to simulate the atomic potential. The metallic nature of the system was confirmed, and the Methfessel−Paxton approximation was used to sample the BZ.[44] A cutoff energy of 600 eV and an 18 × 18 × 1 k-grid were used for the electronic structure calculations. The Grimme-D3 method[45] was used to account for interatomic van der Waals interactions, and the generalized gradient approximation (GGA) functional[46] was used for the exchange-correlation functional. Self-consistent calculations were performed with an electronic threshold of 10^{-6} eV and a convergence criterion of 10^{-3} eV/Å for the Hellmann−Feynman forces.[47]

ASSOCIATED CONTENT

Supporting Information

The Supporting Information is available free of charge at https://pubs.acs.org/doi/10.1021/acsnano.4c05398.

Additional experimental details on the growth of the sample and hole-doping result, additional DFT calculations, and details on the tight-binding calculations are included; Figures S1−S14; discussions (Sections 1−5) are included (PDF)

AUTHOR INFORMATION

Corresponding Authors

Jun-Won Rhim − *Department of Physics, Ajou University, Suwon 16499, Korea; Research Center for Novel Epitaxial Quantum Architectures, Department of Physics, Seoul National University, Seoul 08826, Korea;* orcid.org/0000-0001-9094-0650; Email: jwrhim@ajou.ac.kr

Jongkeun Jung − *Hydrogen·Fuel Cell Research Center, Korea Institute of Science and Technology (KIST), Seoul 02792, Republic of Korea*; Email: jjk3341@gmail.com

Gunn Kim − *Department of Physics and HMC, Sejong University, Seoul 05006, Republic of Korea; Center for Theoretical Physics (CTP), Seoul National University, Seoul 08826, Republic of Korea*; Email: gunnkim@sejong.ac.kr

Changyoung Kim − *Center for Correlated Electron Systems, Institute for Basic Science, Seoul 08826, Republic of Korea; Department of Physics and Astronomy, Seoul National University, Seoul 08826, Republic of Korea;* orcid.org/0000-0003-0555-2341; Email: changyoung@snu.ac.kr

Authors

Jae Hyuck Lee − *Center for Correlated Electron Systems, Institute for Basic Science, Seoul 08826, Republic of Korea; Department of Physics and Astronomy, Seoul National University, Seoul 08826, Republic of Korea;* orcid.org/0000-0001-5341-8652

Gwan Woo Kim − *Department of Physics and HMC, Sejong University, Seoul 05006, Republic of Korea*

Inkyung Song − *Center for Correlated Electron Systems, Institute for Basic Science, Seoul 08826, Republic of Korea*

Yejin Kim − *Department of Physics, Jeonbuk National University, Jeonju 54896, Republic of Korea*

Yeonjae Lee − *Center for Correlated Electron Systems, Institute for Basic Science, Seoul 08826, Republic of Korea; Department of Physics and Astronomy, Seoul National University, Seoul 08826, Republic of Korea*

Sung Jong Yoo − *Hydrogen·Fuel Cell Research Center, Korea Institute of Science and Technology (KIST), Seoul 02792, Republic of Korea; Division of Energy & Environment Technology, KIST School, University of Science and Technology (UST), Daejeon 34113, Republic of Korea; KHU−KIST Department of Converging Science and Technology, Kyung Hee University, Seoul 02447, Republic of Korea;* orcid.org/0000-0003-1556-0206

Deok-Yong Cho − *Department of Physics, Jeonbuk National University, Jeonju 54896, Republic of Korea;* orcid.org/0000-0001-5789-8286

Complete contact information is available at: https://pubs.acs.org/10.1021/acsnano.4c05398

Author Contributions

J.H.L. and G.K. contributed equally.

Notes

The authors declare no competing financial interest.

The preprint version of this article can be found on arXiv. An unconventional platform for two-dimensional Kagome flat bands on semiconductor surfaces. *arXiv* **2023**, arXiv:2401.00265. https://arxiv.org/abs/2401.00265 (accessed July 23, 2024).

ACKNOWLEDGMENTS

The work by J.H.L., Y.L., and C.K. was supported by the Global Research Development Center (GRDC) Cooperative Hub Program through the National Research Foundation of Korea (NRF) funded by the Ministry of Science and ICT (MSIT) (Grant No. RS-2023-00258359) and the NRF grant funded by the Korean government (MSIT) (Grant No. NRF-2022R1A3B1077234). G.W.K. and G.K. were funded by the NRF (Grant No. NRF-2020R1A6A1A03043435). J.J. and S.J.Y. were supported by the NRF (Grant No. NRF-2021M3H4A1A02042948). J.-W.R. was funded by the NRF (Grant Nos. NRF-2021R1A2C1010572, NRF-2022M3H3A106307411, NRF-2021R1A5A1032996, and RS-2023-00285390).

REFERENCES

(1) Yin, J.-X.; Lian, B.; Hasan, M. Z. Topological Kagome Magnets and Superconductors. *Nature* **2022**, *612*, 647−657.

(2) Ye, L.; Fang, S.; Kang, M.; Kaufmann, J.; Lee, Y.; John, C.; Neves, P. M.; Zhao, S. Y. F.; Denlinger, J.; Jozwiak, C.; Bostwick, A.; Rotenberg, E.; Kaxiras, E.; Bell, D. C.; Janson, O.; Comin, R.; Checkelsky, J. G. Hopping Frustration-Induced Flat Band and Strange Metallicity in a Kagome Metal. *Nat. Phys.* **2024**, *20*, 610−614.

(3) Rhim, J.-W.; Yang, B.-J. Singular Flat Bands. *Adv. Phys.: x* **2021**, *6*, 1901606.

(4) Jovanovic, M.; Schoop, L. M. Simple Chemical Rules for Predicting Band Structures of Kagome Materials. *J. Am. Chem. Soc.* **2022**, *144*, 10978−10991.

(5) Lin, Z.; Choi, J.-H.; Zhang, Q.; Qin, W.; Yi, S.; Wang, P.; Li, L.; Wang, Y.; Zhang, H.; Sun, Z.; Wei, L.; Zhang, S.; Guo, T.; Lu, Q.; Cho, J.-H.; Zeng, C.; Zhang, Z. Flatbands and Emergent Ferromagnetic Ordering in Fe_3Sn_2 Kagome Lattices. *Phys. Rev. Lett.* **2018**, *121*, 096401.

(6) Ye, L.; Kang, M.; Liu, J.; von Cube, F.; Wicker, C. R.; Suzuki, T.; Jozwiak, C.; Bostwick, A.; Rotenberg, E.; Bell, D. C.; Fu, L.; Comin, R.; Checkelsky, J. G. Massive Dirac Fermions in a Ferromagnetic Kagome Metal. *Nature* **2018**, *555*, 638−642.

(7) Kang, M.; Fang, S.; Ye, L.; Po, H. C.; Denlinger, J.; Jozwiak, C.; Bostwick, A.; Rotenberg, E.; Kaxiras, E.; Checkelsky, J. G.; et al. Topological Flat bands in Frustrated Kagome Lattice CoSn. *Nat. Commun.* **2020**, *11*, 4004.
(8) Kang, M.; Ye, L.; Fang, S.; et al. Dirac Fermions and Flat Bands in the Ideal Kagome Metal FeSn. *Nat. Mater.* **2020**, *19*, 163−169.
(9) Han, M.; Inoue, H.; Fang, S.; John, C.; Ye, L.; Chan, M. K.; Graf, D.; Suzuki, T.; Ghimire, M. P.; Cho, W. J.; et al. Evidence of Two-Dimensional Flat Band at the Surface of Antiferromagnetic Kagome Metal FeSn. *Nat. Commun.* **2021**, *12*, 5345.
(10) Teng, X.; Oh, J. S.; Tan, H.; Chen, L.; Huang, J.; Gao, B.; Yin, J.-X.; Chu, J.-H.; Hashimoto, M.; Lu, D.; Jozwiak, C.; Bostwick, A.; Rotenberg, E.; Granroth, G. E.; Yan, B.; Birgeneau, R. J.; Dai, P.; Yi, M. Magnetism and Charge Density Wave Order in Kagome FeGe. *Nat. Phys.* **2023**, *19*, 814−822.
(11) Lou, R.; Zhou, L.; Song, W.; Fedorov, A.; Tu, Z.; Jiang, B.; Wang, Q.; Li, M.; Liu, Z.; Chen, X.; et al. Orbital-Selective Effect of Spin Reorientation on the Dirac Fermions in a Three-Dimensional Kagome Ferromagnet Fe_3Ge. *arXiv* **2023**.
(12) Xu, Y.; Zhao, J.; Yi, C.; Wang, Q.; Yin, Q.; Wang, Y.; Hu, X.; Wang, L.; Liu, E.; Xu, G.; et al. Electronic Correlations and Flattened Band in Magnetic Weyl Semimetal Candidate $Co_3Sn_2S_2$. *Nat. Commun.* **2020**, *11*, 3985.
(13) Li, M.; Wang, Q.; Wang, G.; Yuan, Z.; Song, W.; Lou, R.; Liu, Z.; Huang, Y.; Liu, Z.; Lei, H.; et al. Dirac Cone, Flat Band and Saddle Point in Kagome Magnet YMn_6Sn_6. *Nat. Commun.* **2021**, *12*, 3129.
(14) Yin, J.-X.; Zhang, S. S.; Chang, G.; et al. Negative Flat Band Magnetism in a Spin−Orbit-Coupled Correlated Kagome Magnet. *Nat. Phys.* **2019**, *15*, 443−448.
(15) Peng, S.; Han, Y.; Pokharel, G.; Shen, J.; Li, Z.; Hashimoto, M.; Lu, D.; Ortiz, B. R.; Luo, Y.; Li, H.; Guo, M.; Wang, B.; Cui, S.; Sun, Z.; Qiao, Z.; Wilson, S. D.; He, J. Realizing Kagome Band Structure in Two-Dimensional Kagome Surface States of RV_6Sn_6 (R = Gd, Ho). *Phys. Rev. Lett.* **2021**, *127*, 266401.
(16) Liu, Z.; Zhao, N.; Li, M.; Yin, Q.; Wang, Q.; Liu, Z.; Shen, D.; Huang, Y.; Lei, H.; Liu, K.; Wang, S. Electronic Correlation Effects in the Kagome Magnet $GdMn_6Sn_6$. *Phys. Rev. B* **2021**, *104*, 115122.
(17) Hu, Y.; Teicher, S. M.; Ortiz, B. R.; Luo, Y.; Peng, S.; Huai, L.; Ma, J.; Plumb, N. C.; Wilson, S. D.; He, J.; Shi, M. Topological Surface States and Flat Bands in the Kagome Superconductor CsV_3Sb_5. *Sci. Bull.* **2022**, *67*, 495.
(18) Sun, Z.; Zhou, H.; Wang, C.; Kumar, S.; Geng, D.; Yue, S.; Han, X.; Haraguchi, Y.; Shimada, K.; Cheng, P.; Chen, L.; Shi, Y.; Wu, K.; Meng, S.; Feng, B. Observation of Topological Flat Bands in the Kagome Semiconductor Nb_3Cl_8. *Nano Lett.* **2022**, *22*, 4596−4602.
(19) Zhang, H.; Shi, Z.; Jiang, Z.; Yang, M.; Zhang, J.; Meng, Z.; Hu, T.; Liu, F.; Cheng, L.; Xie, Y.; et al. Topological Flat Bands in 2D Breathing-Kagome Lattice Nb_3TeCl_7. *Adv. Mater.* **2023**, *35*, 2301790.
(20) Pan, M.; Zhang, X.; Zhou, Y.; Wang, P.; Bian, Q.; Liu, H.; Wang, X.; Li, X.; Chen, A.; Lei, X.; Li, S.; Cheng, Z.; Shao, Z.; Ding, H.; Gao, J.; Li, F.; Liu, F. Growth of Mesoscale Ordered Two-Dimensional Hydrogen-Bond Organic Framework with the Observation of Flat Band. *Phys. Rev. Lett.* **2023**, *130*, 036203.
(21) Tupchaya, A. Y.; Bondarenko, L. V.; Vekovshinin, Y. E.; Yakovlev, A. A.; Mihalyuk, A. N.; Gruznev, D. V.; Hsing, C. R.; Wei, C. M.; Zotov, A. V.; Saranin, A. A. Double-Atomic-Layer Tl-Mg Compound on a Si(111) Surface with Advanced Electronic Properties. *Phys. Rev. B* **2020**, *101*, 235444.
(22) Lin, Y.-H.; Chen, C.-J.; Kumar, N.; Yeh, T.-Y.; Lin, T.-H.; Blügel, S.; Bihlmayer, G.; Hsu, P.-J. Fabrication and Imaging Monatomic Ni Kagome Lattice on Superconducting Pb(111). *Nano Lett.* **2022**, *22* (21), 8475−8481.
(23) Sun, S.; Zhao, S.; Luo, Y. Z.; Gu, X.; Lian, X.; Tadich, A.; Qi, D.-C.; Ma, Z.; Zheng, Y.; Gu, C.; Zhang, J. L.; Li, Z.; Chen, W. Designing Kagome Lattice from Potassium Atoms on Phosphorus−Gold Surface Alloy. *Nano Lett.* **2020**, *20* (7), 5583−5589.
(24) Aizawa, H.; Tsukada, M. First-principles study of Ag adatoms on the Si(111)−$\sqrt{3}\times\sqrt{3}$−Ag surface. *Phys. Rev. B* **1999**, *59* (59), 10923.
(25) Aizawa, H.; Tsukada, M.; Sato, N.; Hasegawa, S. Asymmetric structure of the Si(111)-$\sqrt{3}\times\sqrt{3}$-Ag surface. *Surf. Sci.* **1999**, *429* (429), L509−L514.
(26) Hasegawa, S.; Tong, X.; Takeda, S.; Sato, N.; Nagao, T. Structures and Electronic Transport on Silicon Surfaces. *Prog. Surf. Sci.* **1999**, *60*, 89−257.
(27) Matsuda, I.; Morikawa, H.; Liu, C.; Ohuchi, S.; Hasegawa, S.; Okuda, T.; Kinoshita, T.; Ottaviani, C.; Cricenti, A.; D'angelo, M.; et al. Electronic Evidence of Asymmetry in the Si(111)−$\sqrt{3}\times\sqrt{3}$−Ag Structure. *Phys. Rev. B* **2003**, *68*, 085407.
(28) Chen, L.; Xiang, H. J.; Li, B.; Zhao, A.; Xiao, X.; Yang, J.; Hou, J. G.; Zhu, Q. Detecting Surface Resonance States of Si(111)−$\sqrt{3}\times\sqrt{3}$−Ag with a Scanning Tunneling Microscope. *Phys. Rev. B* **2004**, *70* (70), 245431.
(29) Zhang, H. M.; Uhrberg, R. I. G. Ag/Si(111)$\sqrt{3}\times\sqrt{3}$: Surface Band Splitting and the Inequivalent Triangle Model. *Phys. Rev. B* **2006**, *74* (74), 195329.
(30) Zhang, H. M.; Gustafsson, J. B.; Johansson, L. S. O. Surface Atomic Structure of Ag/Si(111)−$\sqrt{3}\times\sqrt{3}$. *Phys. Rev. B* **2006**, *74*, 201304.
(31) Sweetman, A.; Stannard, A.; Sugimoto, Y.; Abe, M.; Morita, S.; Moriarty, P. Simultaneous Noncontact AFM and STM of Ag:Si(111)-($\sqrt{3}\times\sqrt{3}$)R30°. *Phys. Rev. B* **2013**, *87*, 075310.
(32) Takeda, S. N.; Higashi, N.; Daimon, H. Visualization of In-Plane Dispersion of Hole Subbands by Photoelectron Spectroscopy. *Phys. Rev. Lett.* **2005**, *94*, 037401.
(33) Rhim, J.-W.; Yang, B.-J. Classification of Flat Bands According to the Band-Crossing Singularity of Bloch Wave Functions. *Phys. Rev. B* **2019**, *99*, 045107.
(34) Ma, J.; Rhim, J.-W.; Tang, L.; Xia, S.; Wang, H.; Zheng, X.; Xia, S.; Song, D.; Hu, Y.; Li, Y.; Yang, B.-J.; Leykam, D.; Chen, Z. Direct Observation of Flatband Loop States Arising from Nontrivial Real-Space Topology. *Phys. Rev. Lett.* **2020**, *124*, 183901.
(35) Rhim, J.-W.; Kim, K.; Yang, B.-J. Quantum Distance and Anomalous Landau Levels of Flat Bands. *Nature* **2020**, *584*, 59−63.
(36) Oh, C.-G.; Cho, D.; Park, S. Y.; Rhim, J.-W. Bulk-Interface Correspondence from Quantum Distance in Flat Band Systems. *Commun. Phys.* **2022**, *5*, 320.
(37) Tong, X.; Ohuchi, S.; Sato, N.; Tanikawa, T.; Nagao, T.; Matsuda, I.; Aoyagi, Y.; Hasegawa, S. Electronic Structure of Ag-Induced $\sqrt{3}\times\sqrt{3}$ and $\sqrt{21}\times\sqrt{21}$ Superstructures on the Si(111) Surface Studied by Angle-Resolved Photoemission Spectroscopy and Scanning Tunneling Microscopy. *Phys. Rev. B* **2001**, *64*, 205316.
(38) Hirahara, T.; Matsuda, I.; Ueno, M.; Hasegawa, S. The Effective Mass of a Free-Electron-Like Surface State of the Si(1 1 1)$\sqrt{3}\times\sqrt{3}$-Ag Surface Investigated by Photoemission and Scanning Tunneling Spectroscopies. *Surf. Sci.* **2004**, *563*, 191−198.
(39) Kim, H.; Oh, C.-G.; Rhim, J.-W. General Construction Scheme for Geometrically Nontrivial Flat Band Models. *Commun. Phys.* **2023**, *6*, 305.
(40) Zhang, W.; Wang, H.; Sun, H.; Zhang, X. Non-Abelian Inverse Anderson Transitions. *Phys. Rev. Lett.* **2023**, *130*, 206401.
(41) Hohenberg, P.; Kohn, W. Inhomogeneous Electron Gas. *Phys. Rev.* **1964**, *136*, B864−B871.
(42) Kohn, W.; Sham, L. J. Self-Consistent Equations Including Exchange and Correlation Effects. *Phys. Rev.* **1965**, *140*, A1133−A1138.
(43) Blöchl, P. E. Projector Augmented-Wave Method. *Phys. Rev. B* **1994**, *50*, 17953.
(44) Methfessel, M.; Paxton, A. T. High-Precision Sampling for Brillouin-Zone Integration in Metals. *Phys. Rev. B* **1989**, *40*, 3616.
(45) Grimme, S.; Antony, J.; Ehrlich, S.; Krieg, H. A Consistent and Accurate ab initio Parametrization of Density Functional Dispersion Correction (DFT-D) for the 94 Elements H-Pu. *J. Chem. Phys.* **2010**, *132*, 154104.
(46) Perdew, J. P.; Burke, K.; Ernzerhof, M. Generalized Gradient Approximation Made Simple. *Phys. Rev. Lett.* **1996**, *77*, 3865.
(47) Feynman, R. P. Forces in Molecules. *Phys. Rev.* **1939**, *56*, 340.

https://doi.org/10.1021/acsnano.4c05398
ACS Nano 2024, 18, 25535−25541